A Compton-Suppressed Phoswich Detector for Gamma Spectroscopy

A.T. Farsoni, B. Alemayehu, A. Alhawsawi, E.M. Becker

Oregon State University, Corvallis, OR 97330

A phoswich detector with two scintillation layers has been designed and assembled at Oregon State University. This detector is able to identify and reject Compton events and ultimately reduce the Compton continuum in gamma energy spectra. In this detector, CsI(Tl) crystal is used to primarily detect photoelectric events. The CsI(Tl) crystal is partially surrounded by a BGO crystal layer to capture and identify Compton-scattered photons. Both crystals are optically coupled to a single photomultiplier tube. A real-time, FPGA-based digital pulse shape analysis was developed to discriminate and reject Compton-induced pulses from the CsI(Tl) crystal. All the digital pulse processing functions including pulse shape discrimination analysis, pile-up rejection and energy measurement were implemented in an on-board FPGA device. In this paper, the results of recent measurements using radioactive lab sources will be presented and discussed.

INTRODUCTION

An ideal gamma-ray detector would have a response function with a single well-isolated peak and no associated Compton continuum. In a typical Compton suppression system, to reduce the Compton continuum and consequently increase the sensitivity of the gamma-ray detector, the primary detector is surrounded by a secondary detector and the detection system is operated in anti-coincidence mode [1]. To build highly-efficient Compton suppression systems, the secondary detector is typically chosen from high-density scintillators such as BGO and NaI(Tl) crystals. Compton suppression systems have improved significantly for various applications over the past few decades [2-4]. Although efficient Compton suppression systems have been proposed and employed in various applications, there are still two limiting factors to their usage: complexity and high overall cost.

In this work, to simplify the Compton suppression system, both primary and secondary detectors have been integrated into one single detector: a phoswich detector. A phoswich detector consists of two or more scintillation layers optically coupled to a single photomultiplier tube (PMT). The energy deposition in each layer from incident radiation is then determined via digital pulse shape analysis of the PMT's anode pulses [5-7].

EXPERIMENTAL

Phoswich Detector

The phoswich detector used in this work consists of two scintillation crystals (Fig. 1): a CsI(Tl) crystal to perform gamma-rays spectroscopy and a BGO crystal, surrounding the CsI(Tl) , to identify and reject scattered photons in the CsI(Tl) . The roles of CsI(Tl) and BGO crystals in this phoswich detector are similar to the roles of primary and secondary detectors in a typical Compton suppression system. The BGO crystal is a high-density (7.13 g/cm3) and high-efficiency scintillator and is commonly used in Compton suppression systems. One other advantage of using a BGO crystal in this detector is to shield the CsI(Tl) crystal against background radiation. The decay time of BGO (~300 nsec) is sufficiently different from the decay time of CsI(Tl) (~1,000 nsec), which facilitates our digital pulse shape analysis algorithm in identifying the origin of radiation interactions. With one additional plastic scintillation

layer placed in the front window, the detector was originally designed to measure xenon radioisotopes via beta-gamma coincidence technique [8].
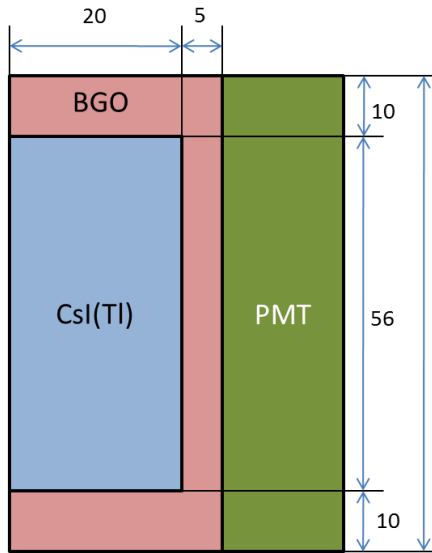

Figure 1: Schematic diagram of the phoswich detector. All dimensions are in mm.
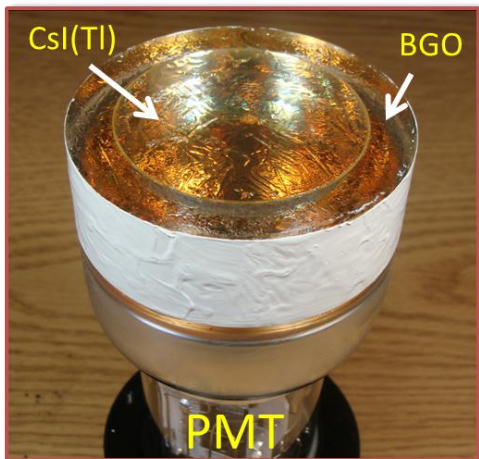

Figure 2: Top view of the Phoswich detector before being wrapped with Teflon tape.

To have flexibility in customizing the phoswich detector, it was assembled in our lab by first smearing a layer of silicone grease (BC-630, Saint-Gobain Crystals) inside the BGO crystal. The CsI(Tl) was then placed inside the

BGO's hole and rotated in order to remove any remaining air bubbles, and uniformly distribute the silicone grease between the crystals, thus forming a good optical coupling. The BGO and the PMT (R1307-07, Hamamatsu) glass window were coupled with a thin layer of silicone grease as well. As depicted in Fig. 2, the side surface of the BGO crystal was covered with reflective paint (BC-620, Saint-Gobain Crystals). The PMT and scintillators were wrapped with 5 layers of Teflon tape and with several layers of plastic wrap. This assembly was then fastened inside a custom built aluminum housing.

Digital Pulse Processing

In this work, a user-programmable digital pulse processor (RX1200, Avicenna Instruments LLC) was used to digitally process anode pulses. The Analog-to-Digital Convertor in RX1200 has maximum sampling rate of 200 MHz and resolution of 12 bits. The RX1200 has an on-board Field-Programmable Gate Array (FPGA) that in normal MCA (Multichannel Analyzer) operation digitally integrates anode pulses and collects an energy histogram in its Block RAM memory (SPARTAN 3, Xilinx Inc.). For our phoswich application, we developed a customized FPGA firmware to perform real-time pulse-shape discrimination and Compton-suppressed gamma-ray spectroscopy.

The current FPGA (150 MHz) firmware has been developed for operation in three modes: (1) Scope mode, (2) MCA mode, and (3) Pulse Shape Analysis (PSA) mode. In the Scope mode, digitized pulse waveforms (1024 samples) are captured and displayed on the PC screen to monitor the performance of whole detection system and to set pulse-capture parameters such as amplification gain, input-offset, ADC-offset and trigger threshold. Digital pulse processing functions such as pulse-shape analysis/discrimination and energy measurement are implemented in the MCA mode. No pulse processing functions are implemented in the PC's user application. In this design, the energy histogram is implemented using 8 x 18kb Block RAMS in the FPGA device. With this configuration, the MCA module collects a gamma energy histogram in 4k (4096) channels with a maximum count of 32 bits (4,294,967,295 counts) per channel. The PSA mode is used to obtain optimum parameters for pulse-shape analysis and discrimination.

Depending on how the gamma-ray interacts with the two scintillation layers in the phoswich detector, three possible pulse-types can be created at the detector anode: (1) single-component pulses from gamma interactions only in CsI(Tl) crystal ("CsI-only" pulses with ~1000 nsec decay time), (2) single-component pulses from gamma interactions only in BGO crystal ("BGO-only" pulses with ~300 nsec decay time), and (3) dual-component pulses from coincidence gamma interactions in CsI(Tl) and BGO crystals ("CsI-BGO" pulses). In our digital pulse processing algorithm implemented in the FPGA device, three main steps are carried out to collect the Compton-suppressed gamma energy spectrum: (A) "CsI-only" pulses are discriminated and captured, (B) captured pulses are digitally integrated to measure the corresponding energy absorption in the CsI(Tl) crystal, and (C) the energy histogram is updated from the pulse integration values.
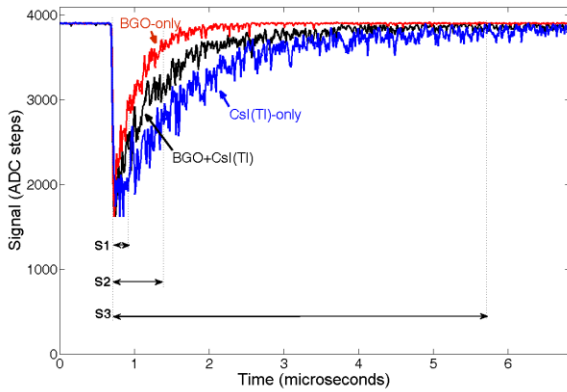

Figure 3: Typical pulses from BGO and CsI(Tl) in the phoswich detector. A combinational (BGO + CsI) pulse due to a coincidence energy deposition (e.g. Compton scattering) in BGO and CsI(Tl) is indicated in black. Three sums (S1, S2, and S3) are calculated and used to discriminate between three different pulse shapes.

To discriminate and identify the above three events, each anode pulse is integrated over three time intervals (Fig. 3). S1, S2 and S3 in Fig. 3 represent the sum of each pulse for 67 ns, 530 ns and 5,000 ns after the trigger point, respectively. Using these sums, two pulse-shape parameters, the Fast Component Ratio (FCR) and Slow Component Ratio (SCR) are calculated from each captured pulse. The FCR and SCR are calculated using the following Equations:

$$FCR = \frac{S1}{S2} \qquad\qquad \text{Eq. 1}$$

$$SCR = \frac{S2 - S1}{S3 - S1} \qquad \text{Eq. 2}$$

Since sum S1 is a fraction of sum S2 and both sums S1 and S2 are fractions of sum S3, the FCR and SCR (Eqs. 1 and 2) range from zero to unity. Fig. 4 shows a two-dimensional scatter plot of the FCR and SCR when the phoswich detector was exposed to a ^{137}Cs source. Three marked regions, shown in Fig.4, correspond to gamma-ray interaction events in BGO, CsI(Tl) or in both crystals (BGO + CsI(Tl)). The "BGO + CsI(Tl)" region is populated from Compton scattering events in CsI(Tl) (or in BGO) and a partial or full energy absorption of scattered photons in BGO (or in CsI(Tl)). The decay time of the CsI(Tl) crystal (~1,000 nsec) is longer than that of the BGO (~300 nsec). This results in smaller FCR and SCR from the CsI(Tl) pulses and places the corresponding events in the "CsI(Tl)-only" region shown in Fig. 4. Having a shorter decay time for the BGO crystal leads to larger FCS and SCR and locate the events in "BGO-only" region. When a coincidence event between the two crystals occurs (e.g. a Compton scattering in one layer and a following interaction in the other layer), the event will be located in the "BGO + CsI(Tl)" region.
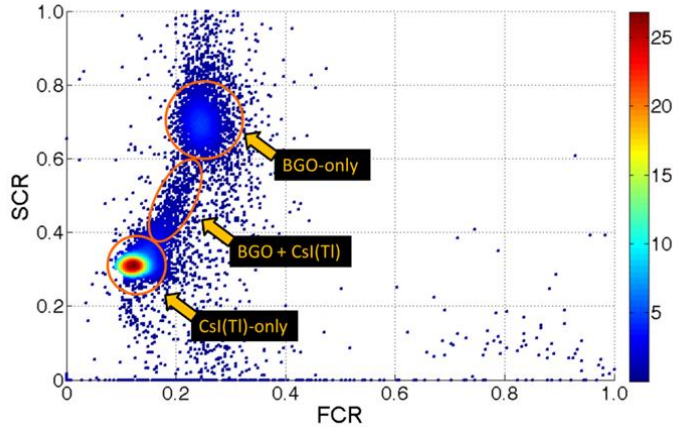

Figure 4: Scatter of the Fast and Slow Component Ratios from [137]Cs. Three marked regions correspond to gamma-ray interaction events in BGO, CsI(Tl) and in both crystals (BGO + CsI(Tl)). The "BGO + CsI(Tl)" region is populated from Compton scattering events in CsI(Tl) (or in BGO) and a partial or full energy absorption of scattered photons in BGO (or in CsI(Tl)).

To evaluate the phoswich detector in suppressing the Compton events in CsI(Tl) and also in rejecting the background radiation, the BGO crystal was removed and measurements were repeated with only the CsI(Tl) crystal in its original place and coupled to the PMT. The same pulse-shape processing algorithm and parameters were employed in both cases. In the following section, the measurement results with and without the BGO crystal are indicated as "suppressed" and "unsuppressed", respectively.

RESULTS AND DISCUSSION

Suppressed and unsuppressed gamma-ray background spectra are presented in Fig. 5. Both spectra were collected for a live time of 9 hours without using shielding. The background rates (20 keV - 2,000 keV range) from suppressed and unsuppressed spectra were measured to be 22.9 and 49.1 counts per second, respectively. This shows a reduction of about 53.3% in the suppressed background rate.
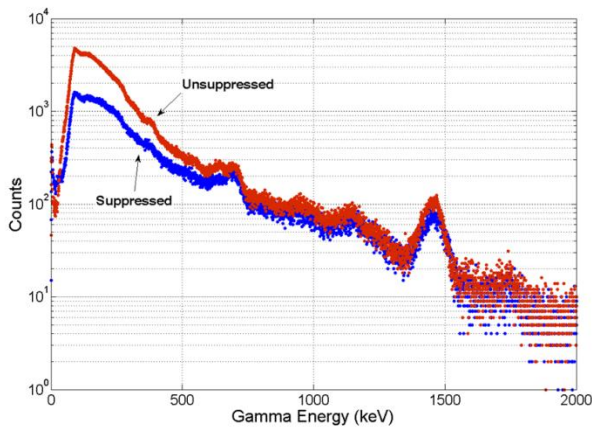

Figure 5: Suppressed and unsuppressed background spectra were collected for 9 hours. No shielding was used in these measurements.

Comparisons between suppressed and unsuppressed spectra from ^{137}Cs and ^{60}Co are presented in Fig. 6. In all measurements, the source and phoswich detector were placed in a 1-inch thick lead shield. In the unsuppressed spectrum, before collecting the spectrum, the amplification gain was reduced to match the photopeak channel number with that of the suppressed spectrum. Without gain matching, due to higher light collection efficiency in the

unsuppressed configuration (without BGO), the spectrum is shifted into higher channels. In spectra shown in Fig. 6, collection of unsuppressed spectra was terminated when the number of counts at the photopeak channel (662 keV in ^{137}Cs and 1.172 MeV in ^{60}Co) reached that of the suppressed spectra. Spectra in Fig. 7-a shows two peaks in the low-energy region: a 30 keV x-ray peak from [137m]Ba and a 78 keV characteristic x-ray peak from the lead shield. By checking Fig. 6-a, we see that Compton events close to Compton edge (340 keV to 477 keV) are more populated in the suppressed spectrum than in unsuppressed spectrum. We believe this is due to the resolution differences between the two spectra. Because both spectra were collected for the same number of counts at the peak channel (662 keV) and since the suppressed spectrum has a poorer resolution (7.9% vs 7.5% for the unsuppressed spectrum), we expect to have a smaller peak-to-Compton ratio for that region. In fact, because large-angle scattered photons from CsI(Tl) have higher chance to escape the detector in both configurations, we should have seen almost the same level of Compton continuum in that energy region. We can see the same situation in Fig. 6-b for [60]Co. Another method for measuring the level of Compton suppression was to collect both spectra with the same number of counts in the photopeak area.
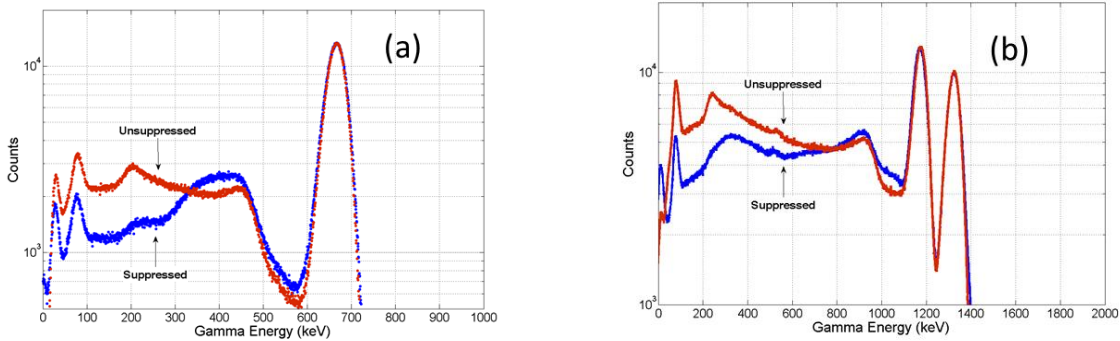

Figure 6: Suppressed and unsuppressed gamma-ray spectra from (a) ^{137}Cs and (b) [60]Co.

To study the Compton suppression mechanism in more detail, the suppression factor was defined as:

$$\text{Suppression Factor (E)} = \frac{C_u(E) - C_s(E)}{C_u(E)} \times 100$$

where $C_u(E)$ is the number of counts in energy E of the unsuppressed spectrum and $C_s(E)$ is the number of counts in energy E of the suppressed spectrum.

8

Fig. 7 shows the resulting suppression factor plot as a function of photon energy using data presented in Fig. 6-a (from 662 keV of ^{137}Cs). Fig. 7 shows that the Compton suppression mechanism for the 662 keV gamma ray is more efficient (30%-58%) in the lower energy region of the Compton continuum (<300 keV) than that of close to the Compton edge. The characteristic shape of the Suppression Factor as a function of energy reflects the fact that because the CsI(Tl) crystal is not surrounded by the BGO crystal at the front window, the BGO is more efficient in detecting small-angle or forward-directed scattered photons from the CsI(Tl) scintillator. Events very close to the Compton edge correspond to large scattering angles and will likely escape the detector without releasing energy in the BGO. The suppression factor of the phoswich detector can be improved by increasing the thickness of the BGO layer. If a maximum window area for the CsI(Tl) is preferred, then the suppression factor can be improved only by increasing the thickness of BGO at the bottom portion (PMT side). Particularly for high-energy gamma rays, this will provide a higher suppression factor since they have strong tendency for forward scattering [1].
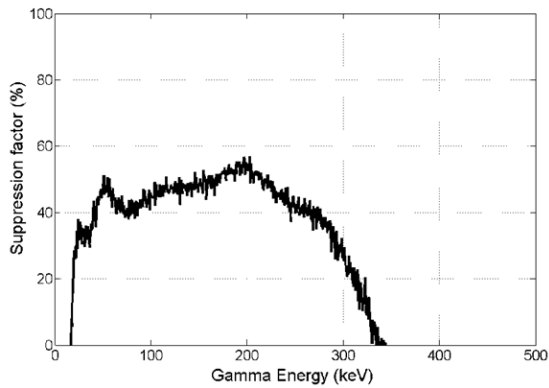

Figure 7: Suppression factor as a function of gamma-ray energy when the detector was exposed to 662 keV of [137]Cs.

Using gamma-ray lab sources, the photopeak intrinsic efficiencies [1] for five photon energies in suppressed and unsuppressed configurations were measured and presented in Table 1. By comparing the photopeak efficiencies given in Table 1, one can evaluate the quality of the pulse-shape analysis method in discriminating and accepting desired events (photoelectric interactions in the CsI(Tl)) in the suppressed configuration. The results show that no significant numbers of photoelectric events are mischaracterized or rejected in the pulse-shape discrimination process.

Table 1: Photopeak efficiencies as measured in the suppressed and unsuppressed configurations.

Photon Energy (keV)	Source	Photopeak Efficiency (%) [Suppressed]	Photopeak Efficiency (%) [Unsuppressed]
344	^{152}Eu	38.33 ± 1.21	39.22 ± 1.24
662	^{137}Cs	17.45 ± 0.54	17.43 ± 0.54
835	^{54}Mn	13.71 ± 0.42	13.04 ± 0.40
1,275	^{22}Na	9.08 ± 0.28	8.5 ± 0.26
1,332	^{60}Co	5.73 ± 0.18	5.47 ± 0.17

Energy resolution of the phoswich detector (in suppressed configuration) was measured for a number of gamma energies. The results are presented in Fig. 8. Energy resolution of 662 keV photopeak from the suppressed and unsuppressed measurements was measured to be 7.9% and 7.5%, respectively. The measured energy resolution in this work for 662 keV was comparable with that of a typical small size (22 mm in diameter and 25 mm long) CsI(Tl) detector [9]. Energy resolution of 1,332 keV photopeak from the suppressed and unsuppressed measurements was measured to be 5.1% and 4.8%, respectively.
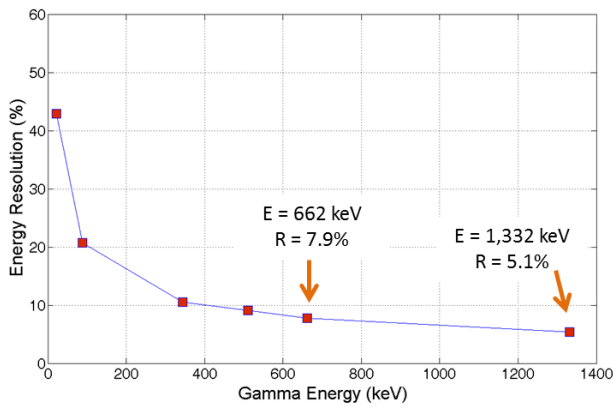

Figure 8: Energy resolution versus gamma energy from suppressed measurements.

CONCLUSION

A phoswich detector with Compton suppression capability was characterized for gamma spectroscopy. In summary, our measurements showed that use of the BGO crystal in this phoswich design and real-time, FPGA-based digital pulse processing have brought two significant improvements in the suppressed gamma energy spectrum: (1) reduction of about 53.3% in background count rate in the energy range of 20-2,000 keV, and (2) up to 58% reduction in the Compton continuum (<300 keV) from 662 keV of ^{137}Cs (for the same number of counts at the photopeak channel). The phoswich detector can be used in gamma spectroscopy applications where a high level of background exists in the energy range of interest, either due to external background radiation or from Compton continuum created from high-energy gamma-rays in the source.

REFERENCES

1. Knoll GF, Radiation Detection and Measurement. 4rd Ed., John Wiley inc., NY, 2010

2. Iskander FY, Landsberger S, Warren SD (2000) J. Radioanal. Nucl. Chem. 244 (1): 159

3. Ishikawa Y, Shoji K, Takahashi M, Watanabe T (2000) J. Radioanal. Nucl. Chem. 243 (2): 367

4. James WD, Boothe PN, Presley BJ (1998) J. Radioanal. Nucl. Chem. 236 (1-2): 261.

5. Ely JH, Aalseth CE, Hayes JC, Heimbigner TR, McIntyre JI, Miley HS, Panisko ME, Ripplinger M, (2003), Proceedings of the 25th Seismic Research Review – Nuclear Explosion Monitoring: LA-UR-03-6029, (V2) 533.

6. Farsoni AT, Hamby DM (2007), Nucl Instrum Methods Phys Res A 578:528

7. Hennig W, Warburton WK, Fallu-Labruyere A, Sabourov K, Cooper MW, McIntyre JI, Gleyzer A, Bean M, Korpach EP, Ungar K, Zhang W, Mekarski P (2009) J. Radioanal. Nucl. Chem. 282 (3): 681

8. Farsoni AT, Alemayehu B, Alhawsawi A (2011), submitted to the IEEE Trans in Nucl Sci.

9. Dolev E, Manor A, Brandys I, Tirosh D, Ziskind G, Orion I (2008), IEEE Trans in Nucl Sci. 55(3): 1237